Plasmonic-based Imaging Detection of Chemical Reactions

by

Yen-Chun Chao

A Thesis Presented in Partial Fulfillment
of the Requirements for the Degree
Master of Science

Approved April 2013 by the
Graduate Supervisory Committee:

Nongjian Tao, Chair
Shaopeng Wang
Tsing Tsow

ARIZONA STATE UNIVERSITY

May 2013

ABSTRACT

An imaging measurement technique is developed using surface plasmon resonance. Plasmonic-based electrochemical current imaging (P-ECi) method has been developed to image the local electrochemical current optically, it allows us to measure the current density quickly and non-invasively [1, 2]. In this thesis, we solve the problems when we extand the P-ECi technique to the field of thin film system. The P-ECi signal in thin film structure was found to be directly proportional to the electrochemical current. The upper-limit of thin film thickness to use the proportional relationship between P-ECi signal and EC current was discussed by experiment and simulation. Furthermore, a new algorithm which can calculate the current density from P-ECi signal without any thickness limitation is developed and tested. Besides, surface plasmon resonance is useful phenomenon which can be used to detect the changes in the refractive index near the gold sensing surface. With the assistance of pH indicator, by applied EC potential on the gold film as the working electrode, the detection of H_2 evolution reaction can be enhanced. This measurement technique is useful in analyzing local EC information and H_2 evolution.

ACKNOWLEDEMENTS

I would like to thank my family for their support. I also thank my advisor, Dr. Nongjian Tao, for his continued support, encouragement, and guidance. I would like to thank other committee members, Dr. Shaopeng Wang and Dr. Tsing Tsow, for their advice on the thesis. It has been a valuable experience in Dr. Tao's group. The helpful discussions with Dr. Xiaonan Shan and other group members are also acknowledged. Thanks to staffs in CSSER for technical suggestions on fabrication process.

TABLE OF CONTENTS

Page

Page

LIST OF TABLES

Table Page

LIST OF FIGURES

Figure Page

Figure Page

Figure Page

CHAPTER 1 Introduction

Since the ability to detect refractive index changes within the vicinity of a sensor surface, surface plasmon resonance (SPR) is a label-free and real-time surface sensing technique. Recently SPR attracts a great deal of attention. SPR acts as an optical method is sensitive to changes in refractive index within a couple hundred nanometers of the sensing surface. SPR is useful in applications including kinetics and affinity, chemical reactions, and environmental monitoring. SPR technology and its applications have been developed already and utilized rapidly. The advantages of SPR are label free, real time, versatile, and highly sensitive resulting in the rapid development of SPR. Among these advantages, for detecting biomolecular activities, label-free detection is the most important advantage of SPR. In other words, since SPR is able to rapidly monitor any dynamic process without the need of label, using SPR to probe surface interactions is advantageous.

Electrochemical (EC) method is an extremely powerful analytical tool that has attracted widespread interested in and been used for a wide range of applications.[3-7] Since EC detection has many gratifying advantages, such as high-sensitivity, rapid response, and adaptation for detecting broad range of analytes, it overrides spectroscopic and chromatographic instruments.[8] However, the total EC current of an electrode is unable to provide local reaction information on the electrode surface. Recently, plasmonic-based electrochemical current imaging (P-ECi) technique has been developed for imaging local EC current by detecting the optical signal of the reaction from SPR.[2] The P-ECi technique is based on that the EC current and SPR signal are both related with

the reaction product concentrations near the electrode. The P-ECi method allows us to optically image the EC current quickly (μs to ms) and non-invasively.

Moreover, in recent years, there has been a significant interest in exploiting microfluidic devices for performing on-chip chemical and biochemical reactions.[9, 10] There are many advantages of microfluidic devices over its competitors in terms of small consumption of sample, low cost, high sensitivity, and so on.[11-13] The use of microfluidic devices for EC detection method is very useful due to the ability to integrate several procedures into a single device. [14, 15] Therefore to extend P-ECi technique in microfluidic thin film structure is very important.

The equation to calculate P-ECi current [1] in an EC cell is based on semi-infinite boundary condition, which has constant concentration at infinity distance from working electrode.[16] This condition will not hold anymore in thin film structure where the boundary conditions (concentration on top and bottom electrodes) will be affected due to the structure. For example, if we apply cyclic voltammetry (CV) potential, the boundary conditions change with applied potential all the time in the thin film structure, as shown in Fig. 1(b). Hence, for thin film EC system, it is no doubt that there is a need to develop new equation for P-ECi. In the next sections, a brief description of P-ECi detection is discussed.

CHAPTER 2 Background and Principle

2.1 Surface plasmon resonance

Surface plasmons are quasi-particles describing the oscillation of charge density, according to a solution of Maxwell's equations for a thin film contacting with a dielectric. The plasmons are the quanta of the oscillations of surface charge excited by an external electric field. The propagating wave is bound to the interface of the metallic film/the electric fields and decays exponentially perpendicular to the surface.[17] When an external electric field excites on a plasma boundary, there will be surface charges like a step function (within the screening length of a few Å). Due to the discontinuity seen by the electric field, *p*-polarized light is the only polarization capable of exciting surface plasmons.[18] For *p*-polarized light, the magnetic field component and the tangential electric field component, E_x, are both continuous across the interface assuming a relative permeability of 1, shown in Fig. 2.1. The electric field component perpendicular to the boundary differs because the two media differ in permittivity, but the electric displacement is continuous across the boundary. This will result in a surface charge density at the boundary and allow for excitation of surface plasmons.[17] The surface charge oscillations are localized in z direction within the screening length.[19]

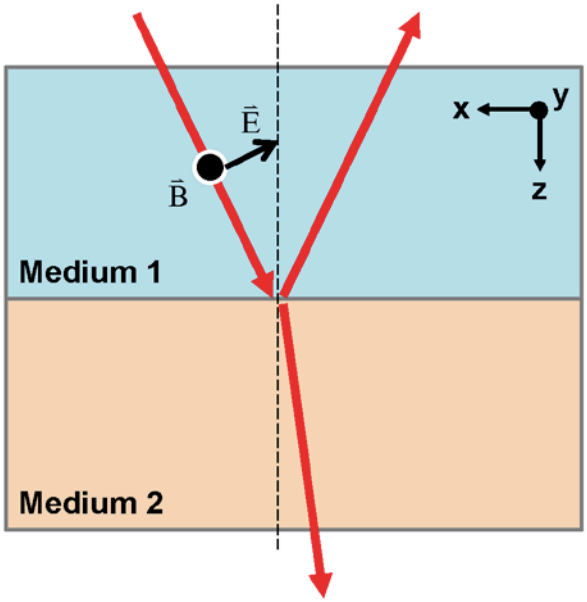

Figure 2.1 Boundary Conditions. For *p*-polarized light, E_z component is discontinuous across the boundary and leads to surface charges on the boundary.

The most popular method to excite surface plasmons is to use light in a total internal reflection mode. The dispersion relation for light is such that it does not normally have the right wavevector and frequency to excite a surface plasmon. Passing the light through a prism at an angle greater than the critical angle required for total internal reflection allows for matching of the wavevector and frequency of the light to that of the surface plasmon at a certain angle of incidence for the incoming light. Two well-known optical setups have been developed for the excitation of surface plasmons: the Otto configuration [20] and the Kretchmann configuration [21] (shown in Fig. 2.2). The Kretschmann setup couples light energy into the metal's plasmons via a metal film on top of a prism. Total internal reflection happens in the prism in the condition that light is reflected through a prism at an angle higher than the critical angle. The Kretschmann configuration is more common than the Otto configuration because of the easier adjustment of surface plasmon properties. The electric field intensity partially extends

beyond the reflecting boundary of the prism and then give rises to an evanescent field. The evanescent field excites the surface plasmons in the metal film with momentum matching conditions.[22] The intensity of coupling can be measured by the change in reflectance of the light from the prism. Especially, at the resonance angle, the light reflectance has its minimum value, as shown in Fig. 2.3. Gold and silver is common metal materials used for the surface plasmon layer because the resonance wavelength is within visible and near-infrared light region. In Kretchmann set up, shown in Fig. 2.2, p-polarized light incident on the interface between the prism and a sensor chip (made by a glass slide coated with a thin metal film). The thickness of metal film should be small enough for the evanescent wave to reach the metal/sample interface (plasma boundary).

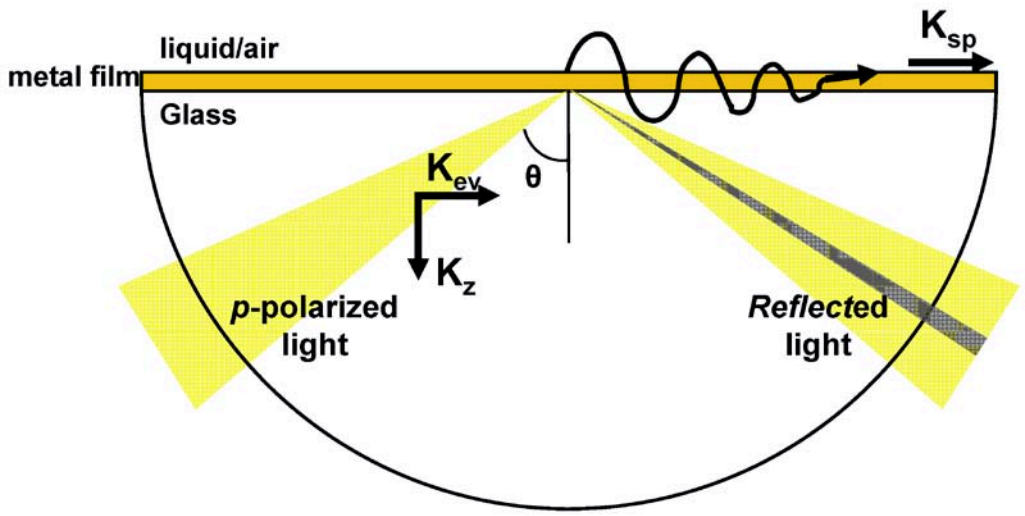

Figure 2.2 Kretschmann SPR setup.

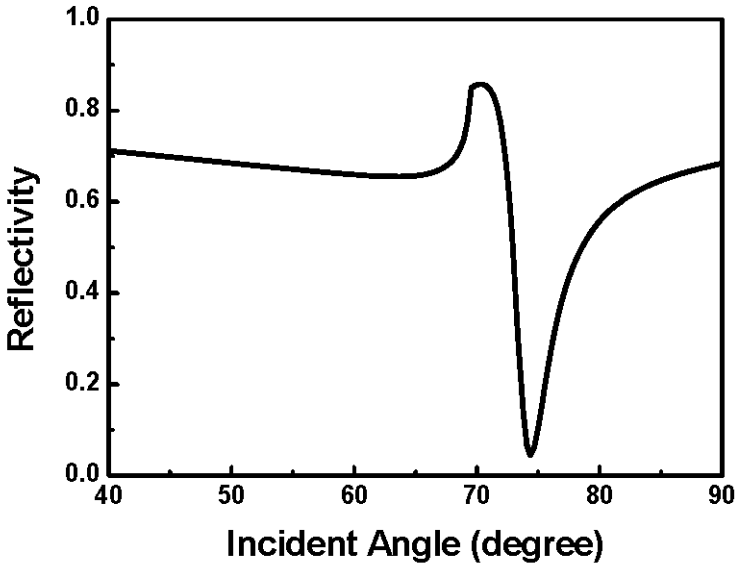

Figure 2.3 SPR curve. At the resonance angle, the light reflectance has its minimum value.

The refractive index of materials contacting with the metal film affect the property of surface plasmon. When the refractive index of sample region changes, the coupling efficiency of the light into the plasmon mode changes. The efficiency can be monitored by observing the surface plasmon coupling angle. The SPR angle mainly depends on the incidence light wavelength, the refractive index of the media on either side of the metal film, and the properties of the metal film. Therefore, the intensity of coupling can be measured by the change in reflectance of the light from the prism. In other words, by fixing the detector at a specific angle within the resonance dip's linear regime, the reflected beam intensity is a linear function of refractive index changing in the testing sample, as shown in Fig 2.4.

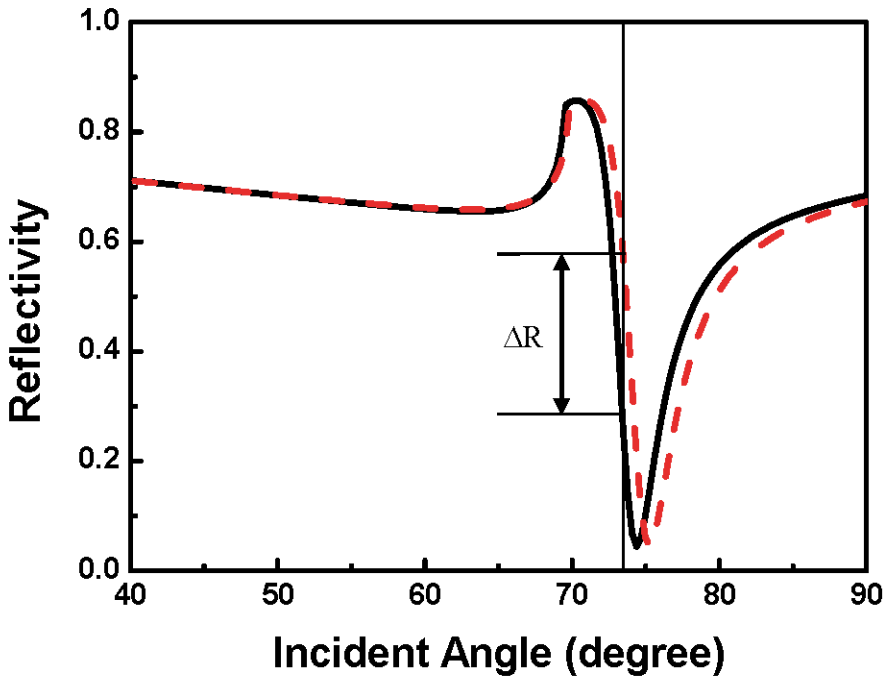

Figure 2.4 SPR curve. Different refractive indexes have different resonance angles. At the fixed incident angle, the reflectivity is a linear function of refractive index changing on the testing sample.

Local information of SPR can be extracted by imaging method. SPR imaging is popular for higher throughput applications. SPR imaging method extracts local information typically from a fixed angle response. Hence, the localized changes in refractive index near the surface can be detected by the localized changes in the reflectance intensity. This imaging capability makes SPR imaging popular for high throughput applications.[23, 24] SPR imaging is a very powerful technique for imaging the surface and is the basis of the method discussed in this thesis.

2.2 Electrochemical measurement

Electrochemistry is concerned with the interrelation of electrical and chemical effects together. Most of this field researches relate with the study of chemical changes resulted from the passage of an electric current and the production of electrical energy by

chemical reactions. From the electrochemical measurement, there are various valuable messages, such as thermodynamic data of a reaction, decay rate of unstable intermediate, and trace amounts of organic species or metal ions. Many electrochemical methods have been well developed and even devised.

Two types of processes occur at electrodes when there is applied potential in the electrochemical cell. In one kind of process, charges (e.g., electrons) are transferred across the interface of metal and solution. Electron transfer results in oxidation or reduction processes. This kind of process is determined by Faraday's law and called Faradaic processes. In other words, the amount of chemical reaction resulted from the flow of current is proportional to the amount of electrons passed. In the other kind of process, non-Faradaic process, although there is no charge crossing the interface, external current flows when the potential changes. This charge flow is caused from adsorption and desorption processes, and the structure change of the electrode-solution interface. Both these two types of processes, Faradaic and non-Faradaic processes, occur when electrode reactions take place. Although Faradaic processes are primary interest in the electrode reaction investigated, non-Faradaic processes have to be taken into consideration in using electrochemical information to probe the charge transfer and associated reactions.

Consider a typical electrochemical experiment, an electrochemical cell is composed of a reference electrode, a counter electrode, and a working electrode submerged in a solution, which in combination are called as a three-electrode setup. Common materials for the working electrode are platinum and gold. The counter electrode can be any material having good conductivity and stability (not react with the bulk solution). The

characteristic of the reference electrode is that the electrode stays at a constant electrochemical potential with respect to the reference potential. A potentiostat is used to control the electrochemical potential of a working electrode. The potential is with respect to a reference electrode. The reference electrode establishes a potential difference between the working electrode and itself. The flowing current flows through the path formed by the counter electrode, working electrode, and solution. Through feedback loop, the potential of the working electrode is adjusted by the current flow from the counter electrode through the solution to the working electrode.

Cyclic voltammetry (CV) is a typical potentiodynamic electrochemical measurement. Any process including electron transfer can be investigated with CV. The working electrode potential ramps linearly versus time. The ramping is the experiment's scan rate (V/s). Take the Fe^{3+}/Fe^{2+} system as an example, the electrochemical reaction is

$$Fe^{3+} + e^{-} \Leftrightarrow Fe^{2+}$$

At the electrode surface, an equilibrium electrochemistry occurs and satisfies the Nernst equation

$$E = E^{0} + \frac{RT}{nF} \ln \frac{[Fe^{3+}]}{[Fe^{2+}]}, \qquad (1)$$

where E is the applied potential difference, and E^0 is the standard electrode potential. The measured current increases as the potential reaches the reduction potential of the analyte. The current increases because the equilibrium position is shifted further to the right hand side and thus converts more reactant. And then the current peak occurs because the diffusion layer is sufficient on the electrode and then the flux of reactant to the electrode

is not fast enough to satisfy the Nernst equation. As a result, useful information, such as the redox potential and electrochemical reaction rates of the compounds, can be obtained.

2.3 Plasmonic-based electrochemical current imaging

As mentioned above, although scanning electrochemical method does has the ability to image local current distribution, the throughput of this method is low and the instrument is complicated. Hence, a high throughput method with the ability to detect local current information is needed. This thesis will discuss this kind of technique called plasmoni-based electrochemical imaging (PECi) technique.

As mentioned in 2.1, SPR imaging technique is an optical method which can observe the local refractive index change near the sensing surface. PECi technique takes advantage of SPR imaging technique and electrochemistry method. It has the ability to image the local electrochemical current on the electrode at a very high throughput (depending on the frame rate, ~ 1000 frames per second). Researches are taken in the PECi fields recently. The first SPR studies of electrochemical reactions was based on detecting local surface potential.[16] There are other approaches based on PECi method, such as detection of surface bound redox species,[25-29] potential-controlled DNA melting, electrochemical polymerization,[30, 31] and detection of metal ions.[26]

When an electrochemical potential applied onto the SPR sensing surface, two main effects will contribute to SPR signal: refractive index change due to the faradaic reaction, and the charge density in the metal film (non-faradaic process). When there is EC reaction in the solution, the refractive index near the SPR surface will change due to the change of redox molecule concentration. In order to demonstrate the principle of PECi,

the relationship between the PECi signal and the faradaic current measured by conventional electrochemical methods is demonstrated below. SPR measures the changes in the bulk refractive index near the electrode. The SPR response, resonance angle shift, can be described by

$$\theta(t) = B\int_0^\infty [\alpha_o C_o(z,t) + \alpha_R C_R(z,t)] e^{-z/l} d(z/l), \qquad (2)$$

where C_o and C_R are the reactant and product concentrations, α_o and α_R are the changes in the local refractive index per unit concentration for the oxidized and reduced molecules, respectively. The constant, B, is the sensitivity of the SPR angle to a change in the bulk refractive index. B can be calibrated for a given SPR setup and reaction species. The exponential term is the decay of the evanesce field from the metal surface into the solution phase. The decay length, l, is ~200 nm.

For a given set of initial and boundary conditions, C_O and C_R can be determined by solving the diffusion equations. Hence, SPR measures local kinetics of product. The ability is suitable for monitoring heterogeneous chemical reactions, taking the advantage of the spatial resolution of SPR imaging.

In the condition of the measurement time scale is slower than the diffuse time of the reaction products over a SPR distance of 200 nm, Eq. 2 can be simplified to

$$\theta(t) = B[\alpha_o C_o(z,t)|_{z=0} + \alpha_R C_R(z,t)|_{z=0}], \qquad (3)$$

where $C_o(z,t)|_{z=0}$ and $C_R(z,t)|_{z=0}$ are the concentrations of the oxidized and reduced molecules near the electrode surface.

In contrast, conventional electrochemical methods measure current density as a function of potential or time,

$$\mathrm{I} = nFD_o \frac{\partial C_o}{\partial z}|_{z=0} = -nFD_R \frac{\partial C_R}{\partial z}|_{z=0}, \qquad (4)$$

where n is number of electrons transferred per electrochemical reaction, F is Faraday constant, D_o and D_{R} are the diffusion coefficients of the reaction species. Comparing Eqs. 2 and 4, both SPR and electrochemical current measurements are both related to the concentration of the reactant and product. SPR detects the concentration changes near the working electrode surface. Electrochemical current measures the concentration gradient on the working electrode. In this respect, SPR gives more direct information about electrochemical reaction than which is measured by current.

In order to get the relationship between SPR signals and current, the concentration profile is critical. Let's take a redox reaction into consideration under one-dimensional (along z-axis) and semi-infinite geometry, by solving the diffusion equation and performing Laplace transform, we can get the relation between concentrations and current density.

$$\mathrm{C_O}(0,t) = C_o^o - [nF(\pi D_o)^{1/2}]^{-1} \int_0^t i(t')(t-t')^{-1/2} dt', \qquad (5)$$

$$C_R(0,t) = C_R^o - [nF(\pi D_R)^{1/2}]^{-1} \int_0^t i(t')(t-t')^{-1/2} dt', \qquad (6)$$

Substituting Eqs. 5 and 6 into Eq. 3,

$$\Delta\theta(t) = \theta_0 + B(\alpha_R D_{\mathrm{R}}^{-1/2} - \alpha_O D_{\mathrm{O}}^{-1/2})(nF\pi^{1/2})^{-1} \int_0^t i(t')(t-t')^{-1/2} dt', \qquad (7)$$

Eq. 7 describes a quantitative relation between the PECi signal and the electrochemical current density measured by conventional electrochemical methods. The PECi signal is a convolution function of the current. SPR signal can be calculated from current and also current can be calculated from SPR signal.

Another non-faradaic current (charging current) is also contributed to the SPR signal in some conditions, such as high concentration of buffer or solution and no electrochemical reaction in solution. When metal electrode surface contacts an aqueous solution including electrolyte, electrical double layer is formed due to the differences in electron affinities of the surface and the solution. When there is potential applied on the metal film, the potential changes the charge density in the electrical double layer. The change of surface charge causes a change in the resonance angle. The relation is shown as below:

$$\Delta\sigma = \alpha\Delta\theta \qquad (8)$$

where

$$\alpha = -\frac{ed_m n_e \varepsilon_2 (\varepsilon_1 + \varepsilon_m)^2 \sin(2\theta_R)}{\varepsilon_1^2 (\varepsilon_m - 1)}, \qquad (9)$$

$\varepsilon_1 = 1.77$ (water), $\varepsilon_2 = 2.29$ (BK7 prism), $d_m = 47$ nm, $n_e = 5.9 \times 10^{-28}$ m^{-3}, $\varepsilon_m = -11.7$ for the gold film, and $\theta_R = 72^o$ according to Eq. 2.

If the background buffer or solution concentration is low, SPR signal due to charging effect can be ignored. The total SPR signal is mostly due to faradaic current. If there is no electrochemical reaction on the surface, the SPR signal is purely due to the charging effect. In other cases, both the faradaic and charging current contribute to the SPR signal.

CHAPTER 3 Thin-film Plasmonic-Based Electrochemical Current Imaging Technique

3.1 Introduction

Electrochemical detection is a powerful analytical method being used for a wide range of applications. For example, DNA and protein detections, trace chemical analysis, glucose and neurotransmitter monitoring, and electrocatalysis studies. Conventional electrochemical measurement gives the total electrochemical current or other electrical quantities of an electrode. However, conventional method does not provide local reaction information of the electrode surface which is critically needed for many applications, such as local activities of cells, and protein and DNA microarrays. Scanning electrochemical microscopy [32] can overcome this limitation by probing local electrochemical current via scanning a microelectrode across the surface.

The equation to calculate P-ECi current [1] in an EC cell is based on semi-infinite boundary condition, which has constant concentration at infinity distance from working electrode,[16] as shown in Fig. 3.1(a). This condition will not hold anymore in thin film structure where the boundary conditions (concentration on top and bottom electrodes) will be affected due to the structure. For example, if we apply cyclic voltammetry (CV) potential, the boundary conditions change with applied potential all the time in the thin film structure, as shown in Fig. 3.1(b). Hence, for thin film EC system, it is no doubt that there is a need to develop new equation for P-ECi.

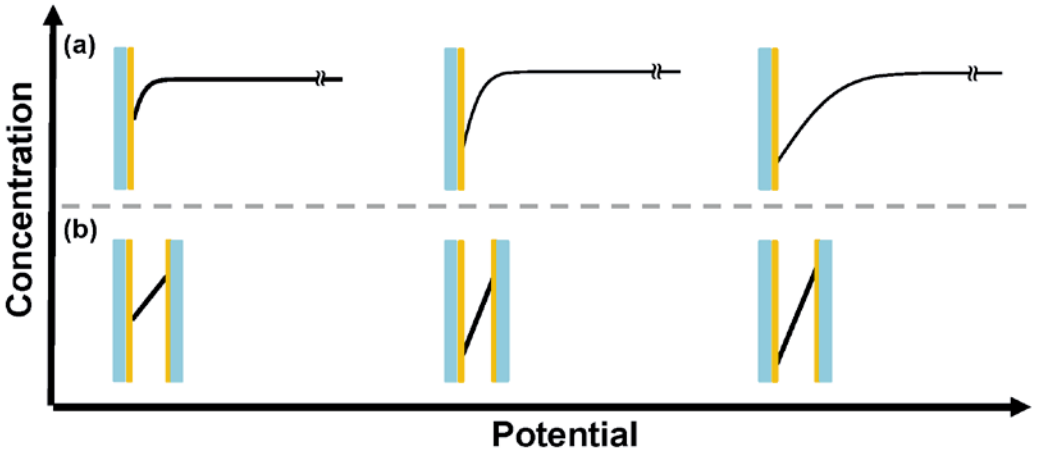

Figure 3.1 Schematic illustration. Concentration profiles with changing potential for the (a) thicker and (b) thinner thin film structures.

In this work, thickness-controlled thin film microfluidic structures with gold electrodes on both top and bottom micro-channel surface were fabricated with poly(dimethylsiloxane) (PDMS) gasket. First, a simulation has been used to demonstrate the SPR signal is proportional to the EC current in thin film microfluidic system. Then, conventional CV current and P-ECi signal have been simultaneously recorded, which demonstrates the P-ECi signal is proportional the EC current in thin film system (25μm and 40μm). Different thickness of thin film systems have been measured, we found that at 0.2V/s scan rate, when the thickness is thicker than 110um the linear relation between P-ECi signal and EC current will not hold any more. To overcome this limitation, an algorithm has been developed to calculate current from P-ECi signal. At the end, the critical scan rate and thin film thickness is discussed.

3.2 Experiment

3.2.1 Reagents

All chemicals were purchased from Sigma-Aldrich and were used without further purification. The 0.2 M sodium fluoride (NaF) solutionwas prepared in deionized water (18 MOhms.cm). The 0.5, 2, 5 and 10 mM ferricyanide/ferrocyanide ($Fe(CN)_6^{3-/4-}$) solutions were prepared by dissolving the 1:1 molar ratio of $Fe(CN)_6^{3-}$ and $Fe(CN)_6^{4-}$ in the prepared NaF solution.

3.2.2 Instrumentation

We used the prism-based SPR imaging setup [33-36] for all experiments described in this article. Prism-based SPR system has been discussed in the literatures we published previously [1, 35, 36]. In short, a collimated p-polarized red LED (Hamamatsu L7868-01) was used as light source and pass through a BK7 prism and shine onto the bottom of the thin film structure. A gold-coated microscope coverslip was placed on top of the prism using index matching oil and used as the SPR sensing surface. The reflected light is imaged by a high-speed CCD camera (Pike F-032B from Allied Vision Technologies, Newburyport, MA 01950).

3.2.3 Preparation of the thin film structure

The 22 × 22 mm no. 1 BK7 glass microscopy coverslips (VWR no. 48366045) were the substrates we used. Prior to the fabrication process, the substrates were cleaned with deionized water and 100 % ethanol. The cleaned coverslips were coated with 1.6 nm of chromium and 47 nm of gold by thermal evaporation (Edwards). The PDMS thin film structures with different thickness were prepared using sol-gel spin coating and thermal

annealing on the top of gold film. The thickness of PDMS thin films was controlled by simple changes in the spin coating rate (i.e., 1000 rpm, 2500 rpm, and 3000 rpm). Finally, the PDMS films were patterned and covered by another gold-coated coverslips as EC wells.

3.2.4 Electrochemical measurement

A potentiostat (microAutolab type III) was used for applying the potential and recording the potential and current. Two electrodes system was applied in thin film structure. For thin film structure, working electrode (WE) is connected to the bottom Au surface which also serves as SPR sensing surface. While reference electrode (RE) and counter electrode (CE) are shorted and connected to the top Au electrode (Fig. 3.2). For EC cell (cut from a flexiPERM 8-well removable and reusable TC Chamber, USA Scientific, Ocala, FL), the cell was placed on top of Au film for holding the reaction solution. Pt wire (CE) and Ag/AgCl (RE) were immersed into the EC cell from the top opening. CV potential is applied in this paper with different potential range. To synchronize the SPR imaging with the EC measurement, the potential and current from the potentiostat is recorded via a national instrument A/D board (NI USB-6210, from National Instruments, Austin, TX 78759) along with the open shutter trigger signal from the CCD camera by a MATLAB program.

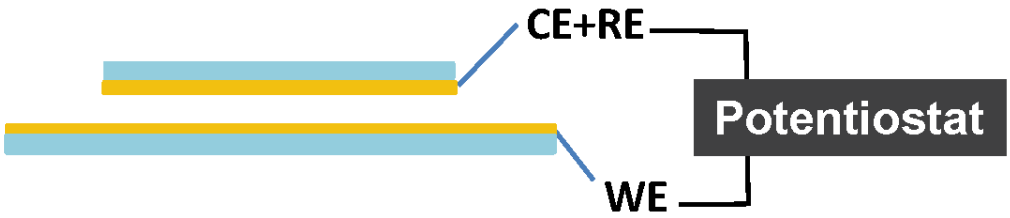

Figure 3.2 Schematic illustration of electrochemical measurement on thin film structure.

3.2.5 Calibration factor

In order to calculate P-ECi current, according to the basic formalism of P-ECi method,[1] we determined the coefficient of current density per SPR angular shift unit. This was carried out by the experiments on different product concentration (2mM, 5mM, and 10mM) for 40-μm-thick thin film structure. There is a linear relation between the conversion coefficient and the measured concentration. The calibration factor was found to be 0.6 A/m^2-mDeg.

3.2.6 Numerical Simulation

To verify our theory, we simulated the concentration distribution and current response numerically. A commercial numerical simulation software COMSOL Multiphysics 4.2 has been used to simulate the concentration profile of redox molecules in thin film with applied potential. Boundary condition is given by Nernst equation:

$$\frac{C_O(0,t)}{C_R(0,t)} = \exp[\frac{nF}{RT}(E(t) - E^0)] \qquad (10)$$

Where R is the molar gas constant, T is temperature, and E^0 is the standard potential. Concentration profile of redox molecules are obtained from diffusion equation and the boundary conditions.

We also develop new algorithm to calculate P-ECi current from SPR response which will not have any thickness limitation on the reaction structure. Since P-ECi signal represents the redox molecule surface concentration, therefore we use P-ECi signal as the boundary conditions of concentrations at all reaction time. By applying this boundary conditions into COMSOL software, we can calculate the concentration gradient on the surface at any time which equals to the current. The current response is simulated by

$$I = nFD_o \left.\frac{\partial C_O}{\partial z}\right|_{z=0} = nFD_R \left.\frac{\partial C_R}{\partial z}\right|_{z=0} \qquad (11)$$

where n is number of electrons transferred per reaction, F is the Faraday constant and Do nad D_R are the diffusion coefficients of the reaction species.

3.3 Simulation

As we discussed in introduction part, the semi-infinite boundary condition will no longer hold in thin film structure, we need to find new relation between surface concentration (proportional to P-ECi signal) and surface concentration gradient (proportional to current). To find out this relationship, we simulate the concentration profiles in the thin film at different potentials with COMSOL Multiphysics (see the Numerical Simulation Section). The simulated potential range is from -0.5V to 0.5V. Figure 3.3 shows the simulated concentration profiles with applied potential from 0 to 0.5 V (quarter period of measurement). Note that both concentrations near the electrode and the concentration gradients increase with applied potential. In other words, the concentration gradients on the surface in the thin film structure are proportional to the concentration gradient.

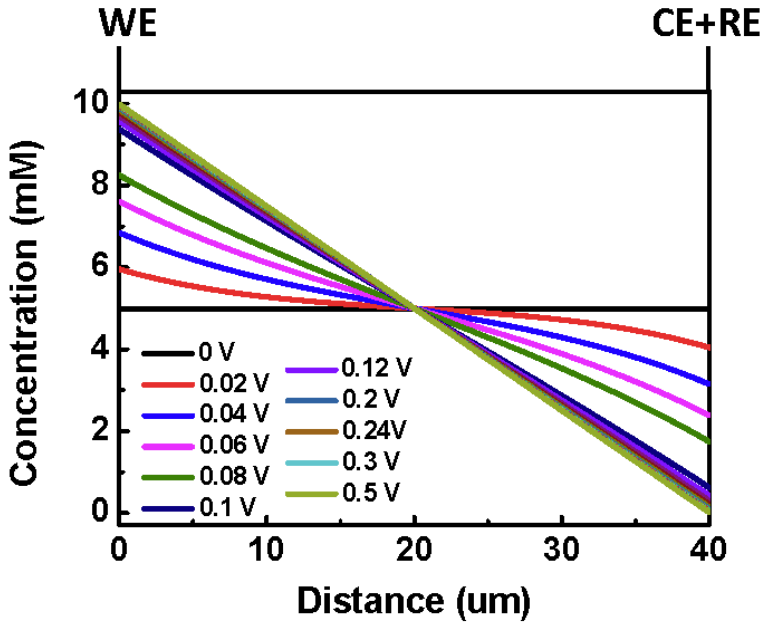

Figure 3.3 Calculated concentration profiles of 40-μm-thick thin film structure.

This is because the diffusion layers of top and bottom electrode overlap when the distance between top and bottom surface is small (less than 80um). The surface concentration at top electrode will directly affect the bottom electrode. When the thickness is small (25um and 40um), the concentration profile between two surfaces is close to straight line (Figure 3.3), therefore the surface concentration gradient or slope is proportional to the surface concentration difference between the top and bottom. Figure 3.4 shows the simulated results of surface concentration gradient and surface concentration for 40-μm-thick thin film structure at different potentials. From the figure we can see that the two curves match perfectly which proves that in the thin film structure, the surface concentration is proportional to the surface concentration gradient. Since the EC current measures the surface concentration gradient on the electrode while P-ECi measures the surface concentration on the electrode, in the thin film structure the P-ECi

signal is directly proportional to the current density. This means that from P-ECi signal we can obtain the local current density of EC reactions without any transformation.

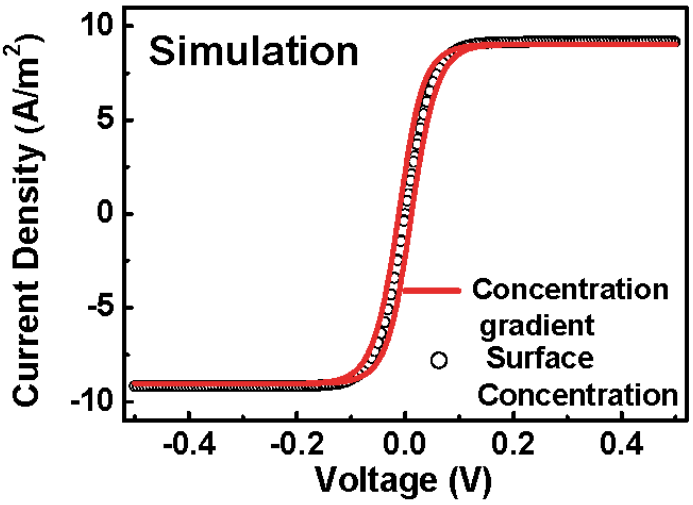

Figure 3.4 Calculated surface concentration gradient (red line) and surface concentration (open circles) with applied potential. The electrode potential sweep from 0 V to 0.5 V with the step of 0.05 V.

3.4 Results and discussion

3.4.1 Different thickness

To prove the linear relationship between P-ECi signal and current density in thin film system, we measured oxidation reduction reaction of $Fe(CN)_6^{3-/4-}$ with conventional CV and P-ECi techniques simultaneously. Since the thin film thickness will affect this relationship a lot, we did experiments on the thin film structures with different thickness (from 10 μm to 110 μm). The thickness is controlled by different spin coating speed of PDMS in fabrication process. Figure 3.5 (a) and (b) show the currents of conventional method and P-ECi method

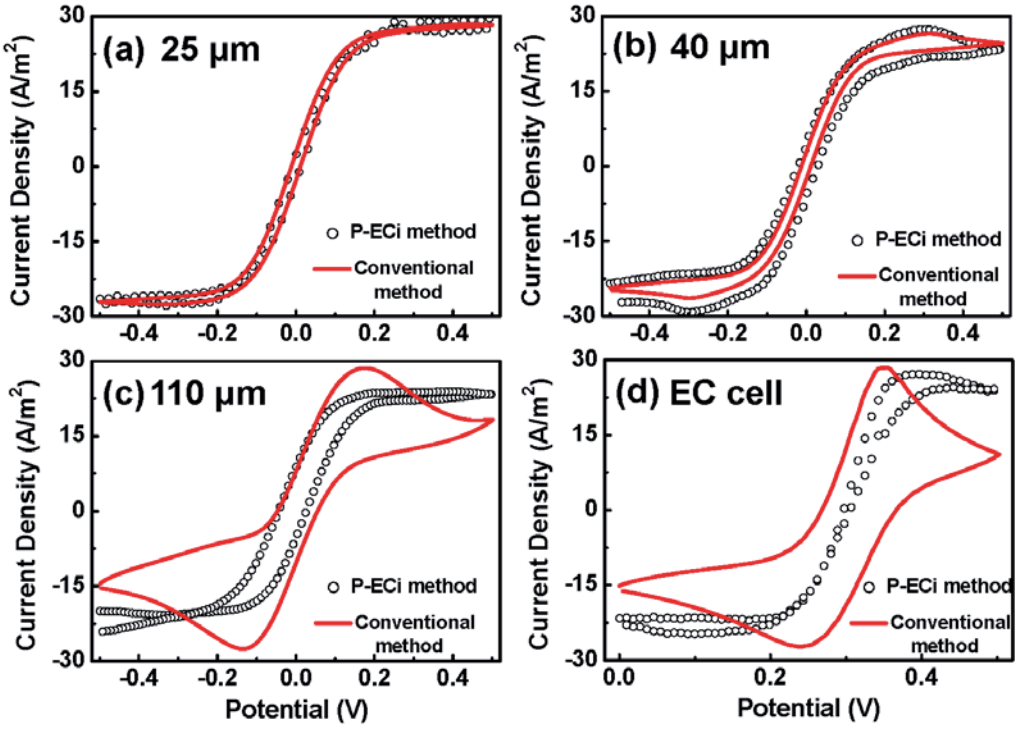

Figure 3.5 Measured CVs by the conventional EC method (red line) and by the P-ECi method (open circles) for (a) 25-μm, (b) 40-μm, (c) 110-μm-thickness thin film structure and (d) EC cell.

versus potential simultaneously. The experiment is carried out in 0.2 M NaF solution containing 10 mM $Fe(CN)_6^{3-/4-}$ in 25 and 40-μm-thick thin film structures, respectively. Note that the P-ECi current is directly obtained from P-ECi signal multiplied by a coefficient (see the Calibration Factor section). The currents obtained by the two methods have high agreement with each other; the overall correlation coefficients for 25 um and 40 um are 0.98 and 0.95 respectively. This proves there is linear relationship between P-ECi signal and current density when thickness of thin film is small (25 um and 40 um). Therefore at 0.2V/s scan rate we can use the equation,

$$I = \begin{cases} \alpha\Delta\theta & , t < 80 \text{ um} \quad (12) \\ bnFL^{-1}[s^{1/2}\Delta\theta] & , t > 80 \text{ um} \quad (13) \end{cases}$$

to calculate the current density in thin film structure, where I is the current density, $\Delta\theta$ is the shift in the SPR signal, α is the coefficient with A/m^2-mDeg (as described in the Calibration Factor section), t is the thickness of thin film structure (the distance between two electrodes), $b = [B(\alpha_R D_R^{-1/2} - \alpha_O D_O^{-1/2})]$, n is the number of electrons involved in the reaction, F is the Faraday constant, L^{-1} is the inverse Laplace transform of the SPR signal. In the expression of b, α_O and α_R are the changes in the local refractive indices per unit concentration for the oxidized and reduced products, D_O and D_R are the diffusion coefficient of the oxidized and reduced products. The selection of thickness condition (80 um) is dependent on the diffusion coefficient and the scan rate of measurement potential. The different scan rate situation will be discussed in the last section.

To further explore the boundary of validity, we measured the reaction in thicker (110 μm) structure and EC cell system (bulk structure) with both conventional and P-ECi methods. As shown in Fig. 3.5 (c) and (d), the CV currents and SPR voltammograms are not in good agreement anymore. The overall correlation coefficient decreases to 0.70 and 0.68, for 110-um-thick structure and EC cell system respectively. The correlation coefficient decreases with increasing thickness. This is because the diffusion layers of top and bottom electrodes begin to separate with increased thickness and the linear relation will not applicable. The CVs and SPR voltammograms are in better agreement with each other for the thinner thin film system, since the surface concentration gradient is in better proportional relation with the surface concentration. This is because the

consumption/generation of $Fe(CN)_6^{3-/4-}$ on top metal electrode is supplemented by the generation/consumption of $Fe(CN)_6^{3-/4-}$ on the bottom electrode immediately. In other words, the product concentration is not constant on the surface of another electrode.

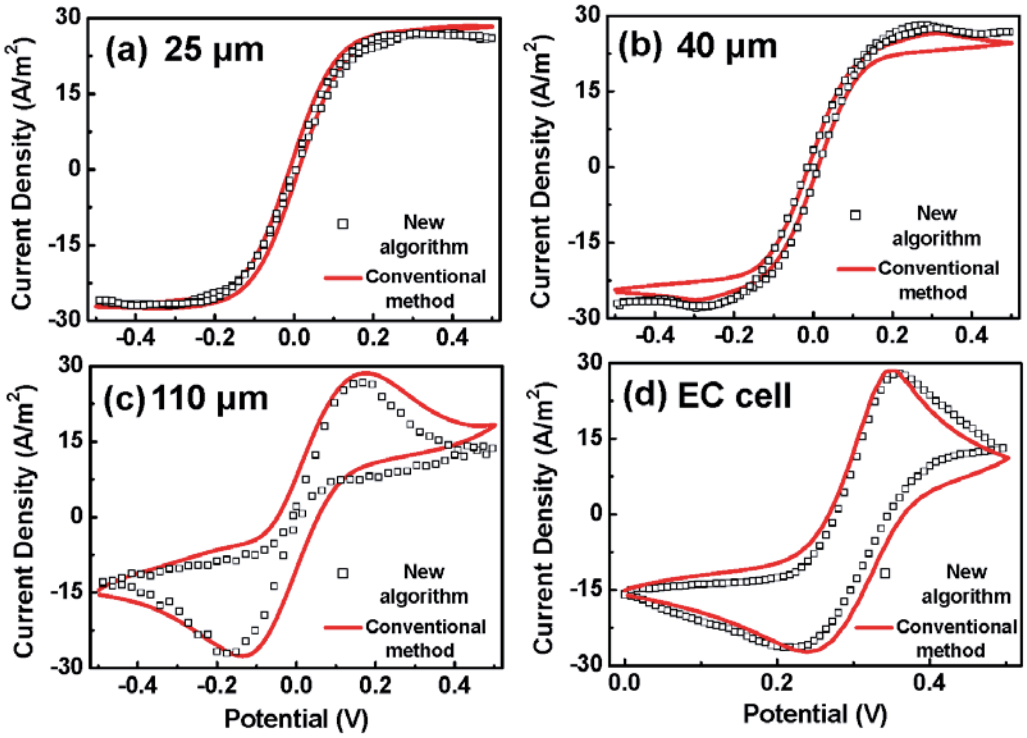

Figure 3.6 Measured CVs by the conventional EC method (red line) and calculated CVs by the new algorithm (open squares) for (a) 25-μm, (b) 40-μm, (c) 110-μm-thickness thin film structure and (d) EC cell.

3.4.2 Universal method

To overcome the thickness limitation, we developed new algorithm to calculate the current density from P-ECi signal. Because the SPR is surface sensitive method, it only measures the concentration within 200 nm from electrode. When the reaction is slower than 1 mili-second [1], the concentration profile within 200 nm could be treated as constant. As a result, in most situations what SPR measured is surface concentration which corresponds to boundary condition of the reaction. Therefore, we converted the P-

ECi signal to surface concentration and applied it into the COMSOL simulator to calculate the concentration profile at any time. From the concentration gradient we can easily calculate the current density. The current density calculated by this algorithm is shown in Figure 3.6. The P-ECi current calculated with the new algorithm have excellent agreement with all the thickness, which prove it is a universal method to calculate P-ECi current.

From the results of Fig. 3.5 and Fig. 3.6, we can see that the relationship between SPR response and CVs varies with the thickness of thin film structures (the distance between working electrode and reference/counter electrode). The different relations are due to the different concentration profiles from different experiment parameters. The concentration profile is related with not only the boundary conditions (surface concentration on the electrodes) but the scan rate of potential sweep. If the diffusion time of $Fe(CN)_6^{3-/4-}$ between two electrodes is shorter than the scan time of quarter cycle of CV measurement, the diffusion layers of the two electrodes affect with each other with applied potential. Figure 3.7 shows the critical scan time for different thickness of channel and diffusion coefficient. Therefore, if the measurement parameters are above the critical scan time curve, we can use Eq. 13 to directly translate between P-ECi signals and CVs. Take our experiments for example, for 25-um-thick (red star) and 40-um-thick (blue star) thin film structure, measured SPR responses can give the local information of EC reactions directly. This figure provides a clear guideline for the method of P-ECi.

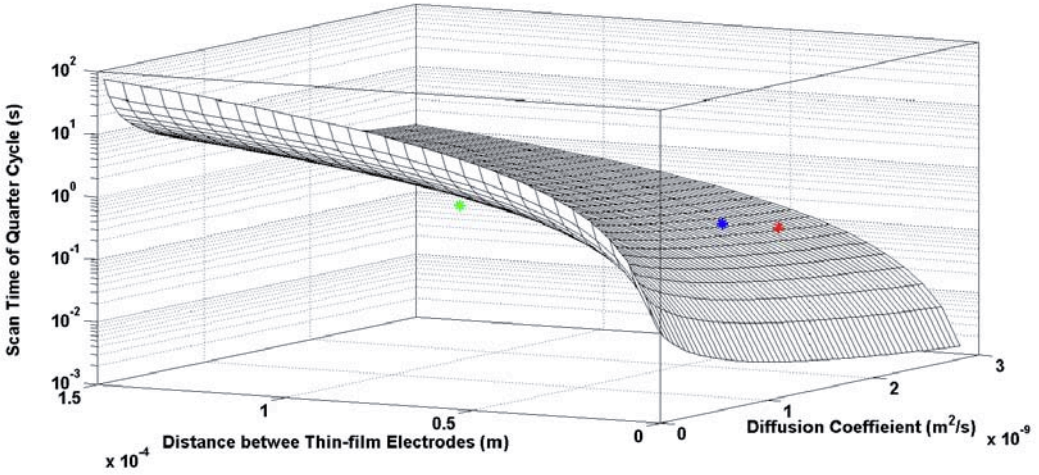

Figure 3.7 For direct PECi, critical scan time of quarter cycle on different conditions (thickness of thin-film channel and diffusion coefficient).

3.5 Conclusion

In conclusion, we have extended the P-ECi method to the thin film structures and developed a universal algorithm to calculate P-ECi current. The situation of thin film structures and traditional EC cell are different due to the different concentration profiles. By numerical simulation and measuring the SPR response and CVs of thin film structures with different thicknesses, it has been unambiguously demonstrated that we can directly track local EC reactions by SPR response when the diffusion layers of the electrodes are overlapped. To overcome the limitation on distance between electrodes, new thickness-independent algorithm can give the P-ECi information from measured SPR response. Systematic discussion on the connection of SPR signals and CVs provides valuable information to strengthen the P-ECi method.

CHAPTER 4 Enhanced H^+ Detection by pH Indicator

4.1 Introduction

Detection of biological and chemical species is a fundamental step to the screening of disease and drugs, as well as biomolecular analysis and gas detection.[37] For instance, the detection of proteins, virus, and DNA, the detection of calcium and potassium ion concentrations in vivo are critical.[38-41] Nanostructures, such as nanowires, nanotubes, and nanoparticles are particularly attractive as biosensors and chemical sensors.[42-44] Nanoparticles have attracted broad interests and numerous applications have been developed over the past two decades. The interested fields are included sensors,[45, 46] optoelectronics,[47] electrocatalysis,[48] and so on. Among these applications, one of the most important areas is the electrocatalysis reaction of nanoparticles.[48, 49] The main reason making nanoparticles popular is the advantage of high surface-to-volume ratios compared with bulk materials. The detection sensitivity is therefore enhanced greatly since the signal can be enhanced due to the large surface-to-volume ratio.

The principle of SPR imaging technique has been demonstrated in Chapter 2 and 3. It has the advantages of mapping local information of an electrode with sub-micron resolution. Instead of probing on sensing surface point by point with microelectrode,[50] SPR imaging technique images the local characteristics optically by measuring the refractive index change near the electrode surface. A pH indicator is a halochromic chemical compound added in small amount into a solution, and the color of the solution changes depending on the pH value. When pH changes in the solution with pH indicators, the refractive index of solution also changes. Combine the advantages of SPR imaging

with the help of pH indicator, the sensitivity of H^+ by SPR imaging technique can be enhanced.

In this chapter, first, to demonstrate the ability of SPR imaging technique for detecting H^+ changes with pH indicator, H^+ detection is investigated by SPR imaging. The detection limit of H^+ by SPR with the help of pH indicator is discussed. In addition, to exam the enhancement of P-ECi for H^+ detection by pH indicator, hydrogen generation reaction by Pt nanoparticle is investigated by P-ECi. Platinum nanoparticle was modified onto Au surface. EC potential is applied on the Au surface, due to the H_2 generates from the Pt nanoparticle area, the refractive index is changed which can be detected by P-ECi. With the assistance of pH indicator, the detection limit of H^+ reaction on Pt nanoparticle is enhanced.

4.2 Experiment

The principle and experimental setup consists of two major components, a three-electrode electrochemical setup and an optical detection system.

Three-electrode electrochemical reaction. A Teflon EC reaction cell is mounted on a BK7 glass slide coverd with 40-nm gold. The Au substrate is used as working electrode, Pt wires is used as counter electrode, and the Ag/AgCl is used as reference electrode. An Autolab potentiostat is used to apply potential to the electrochemical cell for cyclic voltammetry scan.

Optical detection setup. The substrate is placed on a BK7 prism covered with a drop of index matching oil. A p-polarized 670-nm laser beam is incident onto the prism

surface and the reflected beam is detected by a CCD camera. The incident angle was adjusted for a best sensitivity range.

Pt nanoparticle synthesis. Citrate-stabilized platinum nanoparticles are synthesized. A total of 1L of 1 % H_2PtCl_6 aqueous solution was added into 100 mL of DI water and heated to boiling. Then 3 mL of 1% sodium citrate aqueous solution is added quickly into the boiling solution. The mixture is kept boiling for 30 min, until the color of solution turns dark.[104] The size of PtNP is from 10 to 20nm. The Pt nanoparticle solution is dispensed onto Au surface. The droplets dry rapidly. Then the substrate is rinsed with DI water for 10 seconds to rinse out the residue from Pt nanoparticle solutions and nonbinding Pt nanoparticles. N_2 gas is used to dry the substrate.

4.3 Results and discussion

4.3.1 Without applied voltage

Different pH indicator. The position of the color-change interval in the pH value differs widely with different pH indicators. In order to find out the best common laboratory pH indicator for SPR sensing, different pH indicators are tested for their sensitivities to the pH changes. Besides, consider for future applications on biological reaction detection, the pH indicators we took have the transition pH range near the neutral region. We valuate three pH indicators: bromocresol green, phenol red, and 4-nitrophenol. The characteristics of these three pH indicators are shown in Table 4.1. The pH indicator solution concentration is 1 mM in DI water. To change the pH value of the solution, 10 μl 0.25-M H_2SO_4 is added three times and 0.25 μl 0.25-M NaOH is added twenty times into the solution containing different pH indicators. The pH value changed

from 1 to 12. SPR intensity changes are recorded as a function of time with pH value changing, as shown in Fig. 4.2. For bromocresol green, there is an evident SPR intensity change as the pH value changing from 4.50 to 5.00. The pH values are measured. The result of the SPR intensity changing with the pH value for bromocresol green is shown in Fig. 4.3. For phenol red, the SPR intensity increases with increasing pH value in the pH range of 3.60-4.60. For 4-nitrophenol, the SPR intensity keeps increasing from the pH value changing to acid and back to base. From these results, it is clear that bromocresol green has the best intensity of changing pH value in our SPR experiment setup.

Indicator	Low pH color	Transition pH range	High pH color
Bromcresol green	yellow	3.8-5.4	blue
Ethyl red	red	4.4-6.2	yellow
4-nitrophenol	colorless	5.6-7.6	yellow

Table 4.1 pH indicator characteristics.

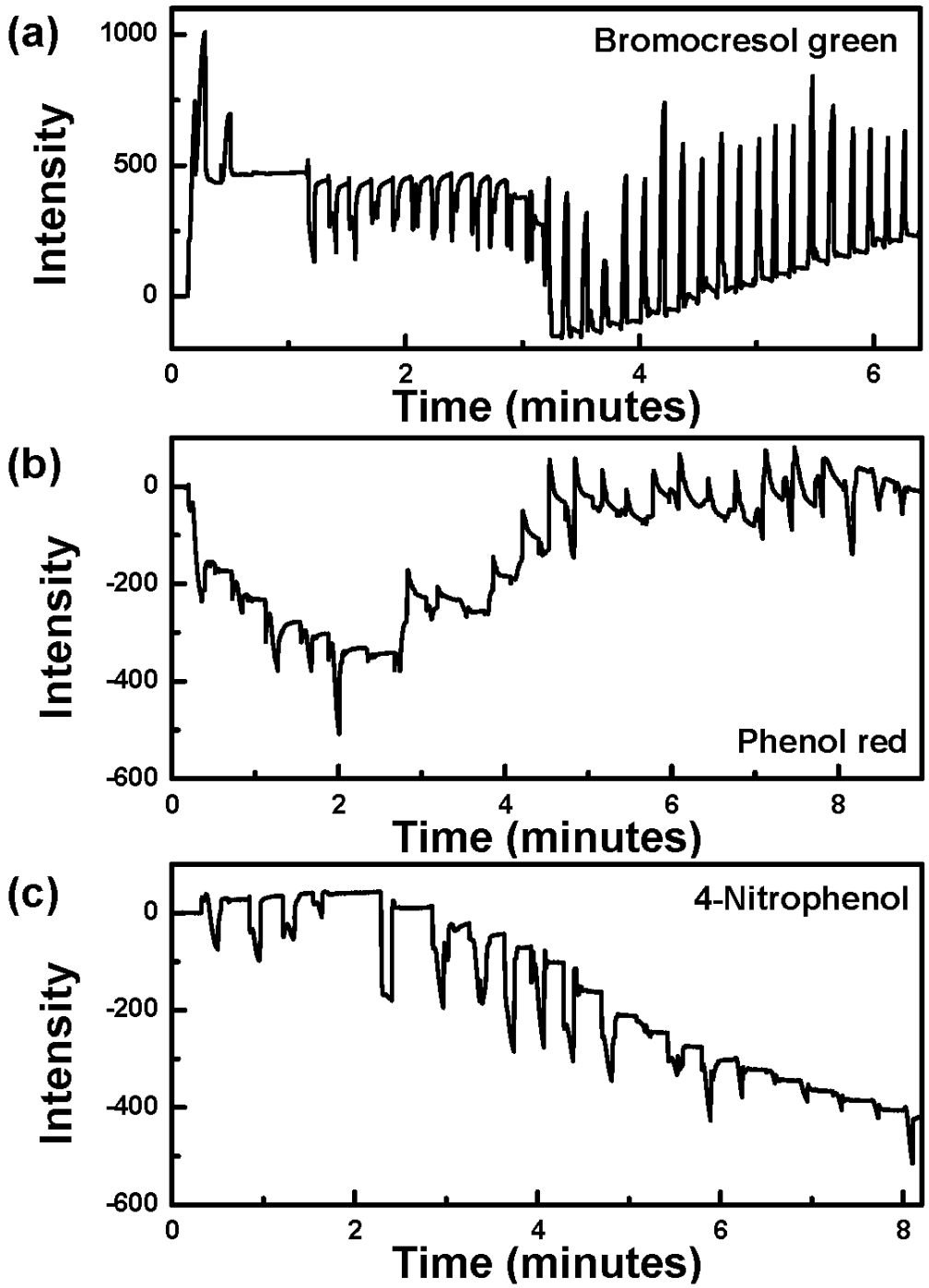

Figure 4.2 SPR intensity changes are recorded as a function of time with pH value changing for different pH indicators: (a) bromocresol green, (b) ethyl red, and (c) 4-nitrophenol.

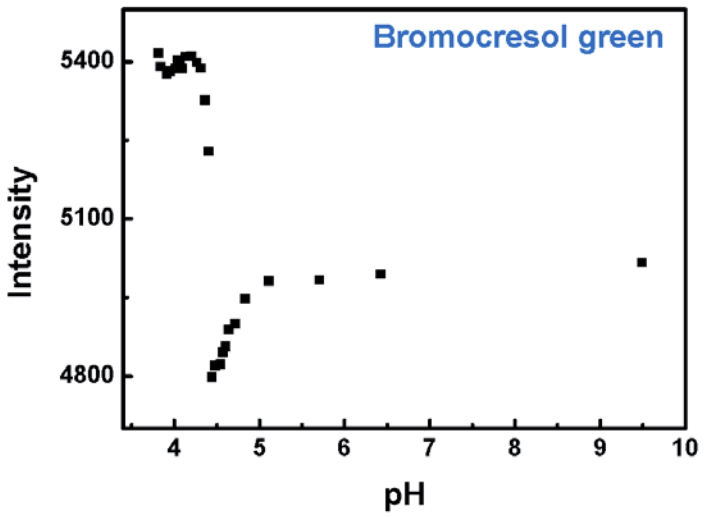

Figure 4.3 SPR intensity changes with pH value for the pH indicator of bromocresol green.

The sensitivity is related with the refractive index (color) change of pH indicator. Hence, for these three pH indicators, absorbance spectra at different pH values are measured. The incidence-light wavelength range is from 500 nm to 820 nm. The light is normal incident into the solution. For bromocresol green, the absorbance has an obvious change at 670 nm (the light wavelength in SPR measurement setup) and the absorbance range moves in the red light region as the pH value changes from 4 to 5, as shown in Fig. 4.4. For phenol red and 4-nitrophenol, the absorbance intensities change at 670 nm, but the absorbance bands keep the same at different pH values, as shown in Fig. 4.5. The absorbance band clearly changes with pH changing for bromocresol green. This results in the highest pH sensitivity by SPR detection due to the match between refractive index change and the light wavelength. Figure 4.6 shows the detection limit for 1-mM bromocresol green as the function of pH value. The detection limit is 180 number/μm^2 when the pH value changes from 4.31 to 4.35.

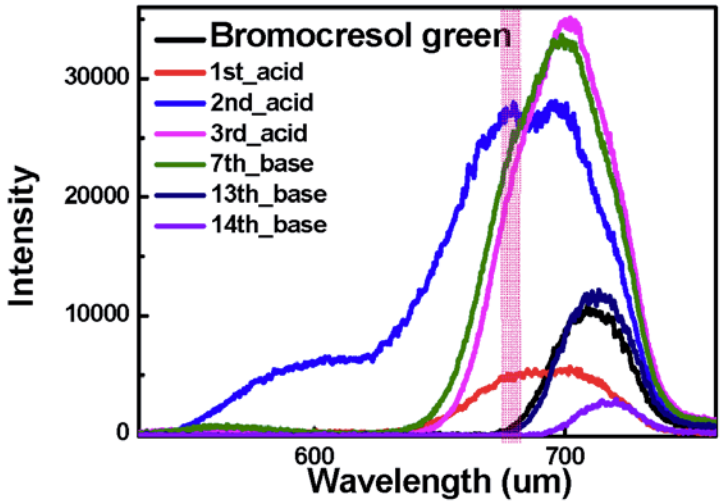

Figure 4.4 Absorbance spectra at different pH value for bromocresol green.

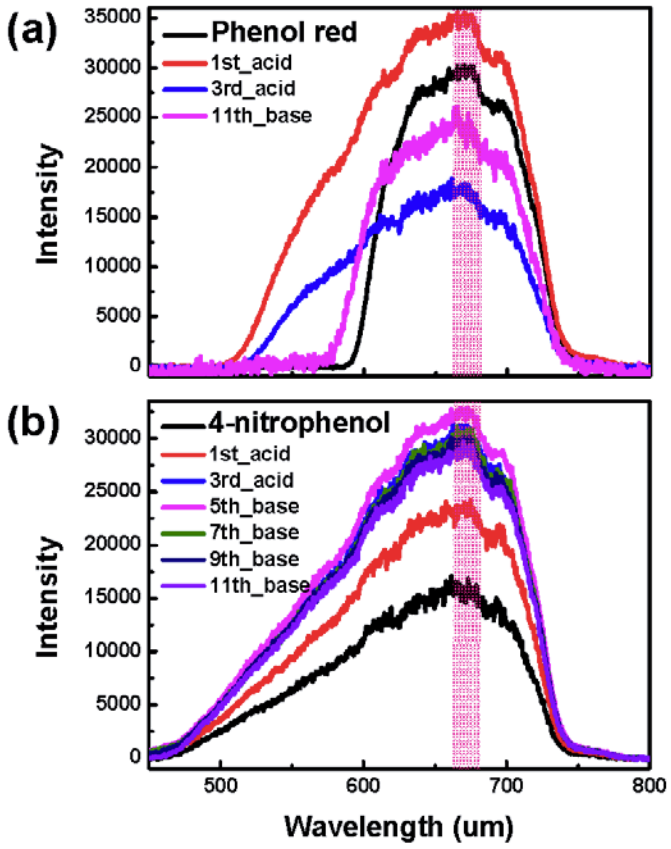

Figure 4.5 Absorbance spectra. For different pH indicator, (a) phenol red and (b) 4-nitrophenol, absorbance spectra at different pH value.

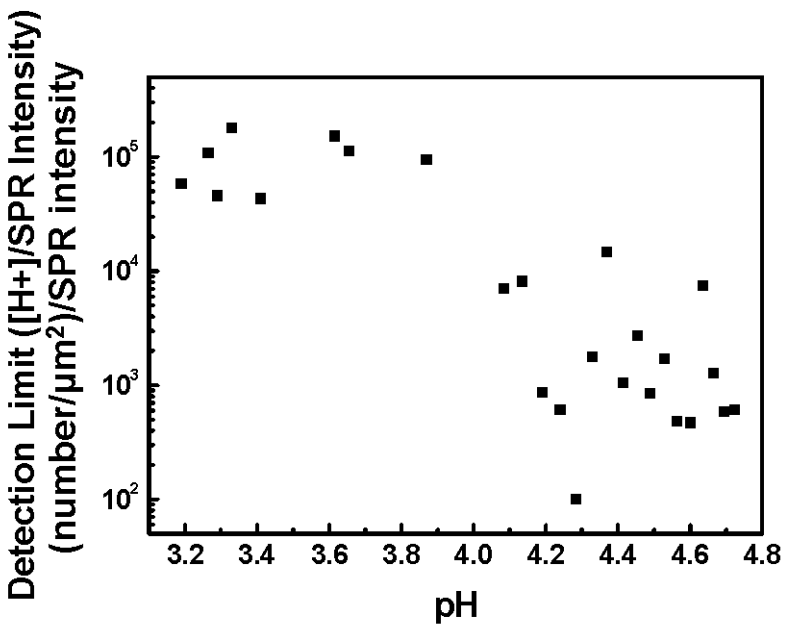

Figure 4.6 The detection limit for 1-mM bromocresol green as the function of pH value.

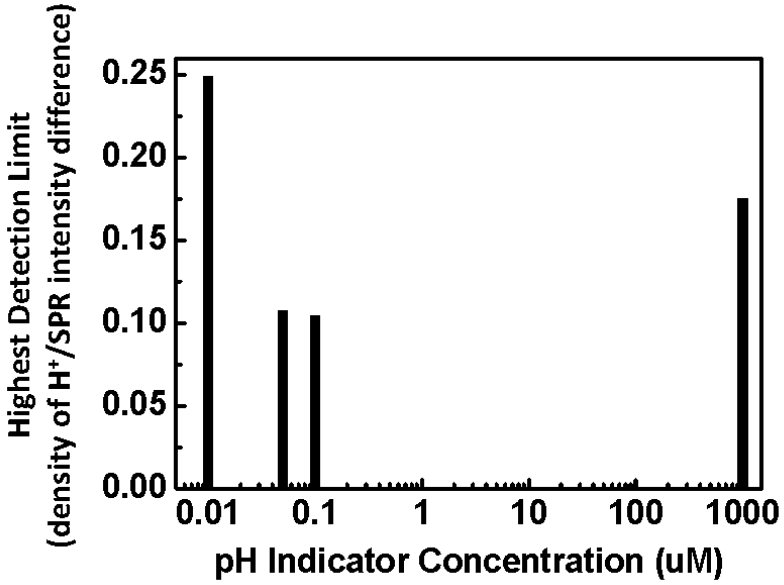

Figure 4.7 The highest detection limit for different-concentration pH indicator.

In order to check whether the concentration of pH indicator affect the detection limit or not, we repeat the experiment on different concentrations of pH indicator, 0.01 μM, 0.1 μM, 0.01 mM, and 1mM. The results are shown in Fig. 4.7. For all the different

concentrations of pH indicator, the detection limit has maximum value as the pH value changes near 4.30. The highest detection limit is 90 (number/μm^2)/SPR intensity occurring with 0.1-μM pH indicator.

4.3.2 With applied voltage

From the previous section results, 0.1-μM bromocresol green performs the best H^+ detection limit. To further investigate the assistance of pH indicators, the hydrogen generation reaction by Pt nanoparticles is investigated by P-ECi. The potential is applied to the patterned Au surface by a three-electrode system as described in experiment section. The Pt nanoparticles are dispensed onto Au surface to form patterned surface. Figure 4.8 shows the SPR image of Pt-nanoparticle patterned Au surface. The ellipsoidal shapes bright patterns represent the Pt nanoparticle area which has higher reflectivity due to the coverage of Pt nanoparticles.

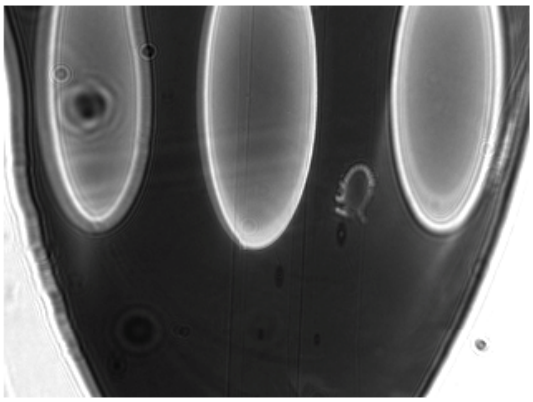

Figure 4.8 SPR image of Pt-nanoparticle patterned Au surface.

First, in order to confirm the suitable applied voltage range for detecting hydrogen generation reaction at different pH values, the experiments taken on purely Au surface without pH indicator. At lower pH value, the hydrogen generation starts to react at lower

applied voltage. When the pH value is 1, there is hydrogen generation on Au surface at ~0.7 V. According to the investigated results shown in the previous section, the interested pH range is 3-5 because the lowest detection limit happened in this range of pH value. The suitable applied voltage range for the next step of the experiment, the P-ECi detection of hydrogen generation reaction on Pt nanoparticle area, is determined by that there is near-zero hydrogen generation on the Au surface at certain pH value. Hence, from the measurement results, for the pH value of 3 and 5, the suitable applied voltage range is from 0.3 V to -0.9 V.

Figure 4.7 shows the typical P-ECi response in which the black curve is the response of Au surface region and the red curve is Pt nanoparticle region. The applied voltage range is from 0.3 V to -0.9 V. The pH value of the solution is ~5. The Au area only shows the typical charging effect response throughout the entire scan. However, the response on Pt nanoparitcle area has much sharper peak at more negative potential (<-0.70 V). This phenomenon is because Pt nanoparticles catalyze the H_2 evolution reaction on its surface at negative potential (<-0.70 V), and thus the refractive index near sensing surface changes due to the generated H_2 molecules on the Pt nanoparticle area. Hence, the P-ECi signal on Pt nanoparticle area decreases more at negative potential while the signal on Au area still governs by charging effect. In other words, the P-ECi signal has much shaper peak when applied potential is more negative than -0.70 V. Without bromocresol green in the electrolyte solution, the P-ECi response of Pt nanoparticle and Au region is almost the same.

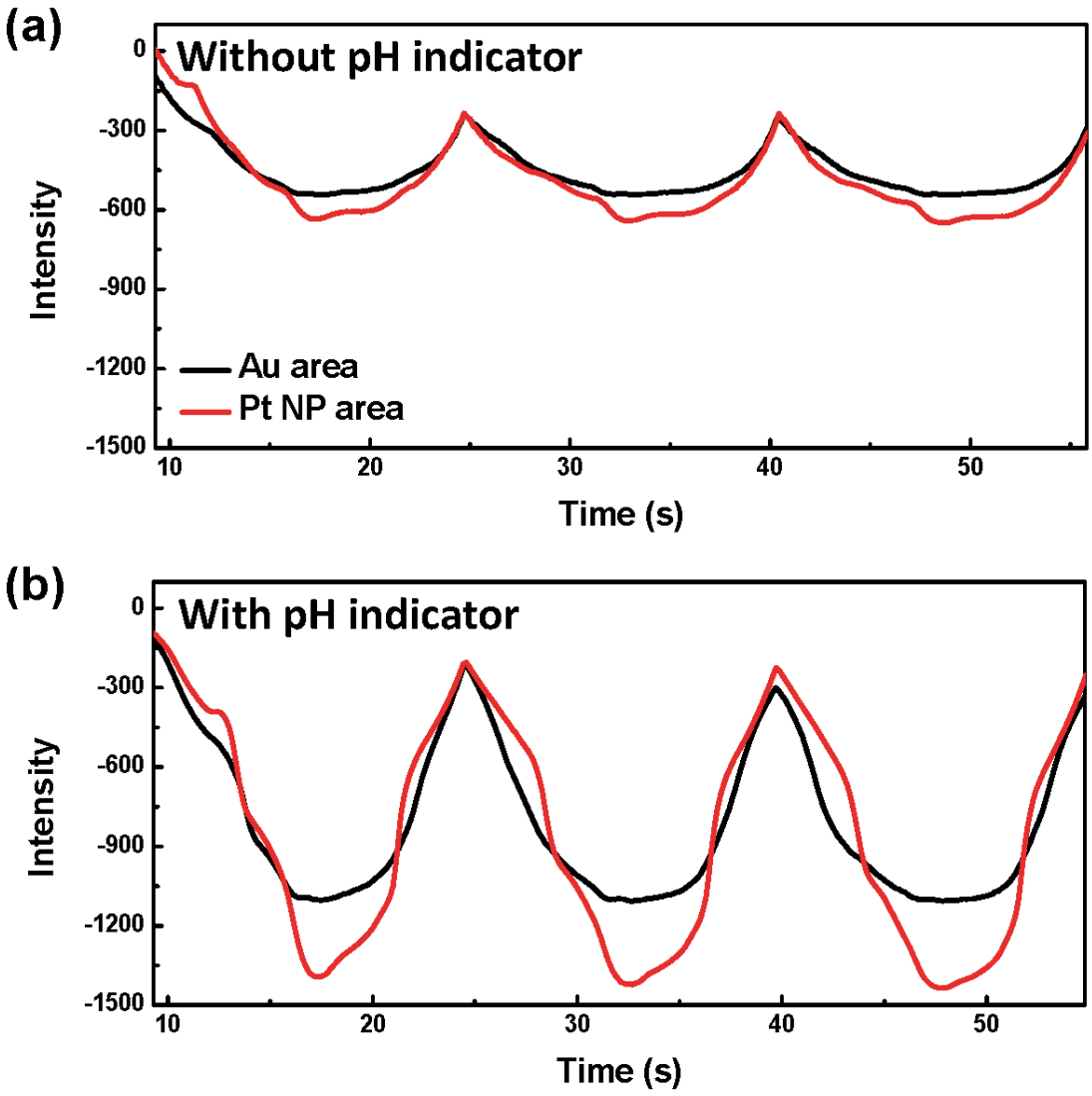

Figure 4.9 P-ECi response of different region for 3 CV scan cycles (a) without and (b) with pH indicator in solution. Black curve: Au surface region, red curve: Pt nanoparticle region, and blue curve is the response difference between Pt nanoparticle and Au region.

By adding bromocresol green into the electrolyte solution, the responses of both Au and Pt nanoparticle regions are enhanced, as shown in Fig. 4.9(a). In other words, with the assistance of pH indicator, the P-ECi detection of hydrogen generation reaction (pH value increases) can be enhanced. Note that the H_2 molecules generated from surface are dissolved in solution, and it does not nucleate until certain high concentration is reached.

In the case of our experiment case, as long as the potential is higher than certain value, the generated H_2 molecule can diffuse away before the concentration increases to the limit to trigger the nucleation. Figure 4.10 shows the comparison of with and without pH indicator in the solution for Au and Pt nanoparticle area. The enhancement by pH indicator for Au area and Pt nanoparticle area is 2.03 times and 2.33 times, respectively.

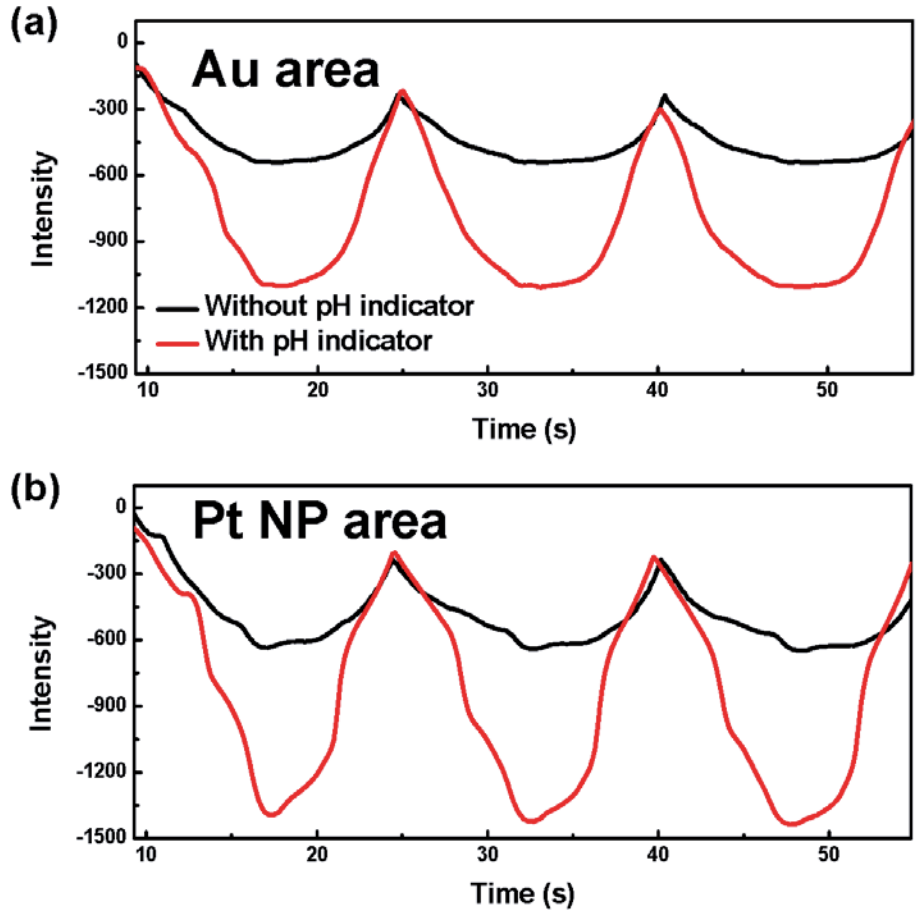

Figure 4.10 The enhanced detection of Pt nanoparticle catalytic reaction measured by P-ECi method.

According to the principle of P-ECi method, the detection is related with the concentration profile near the sensing surface. The concentration profile is determined by the generation and diffusion processes. Hence, the experiment's scan rate also affects the

detection. There must be room for improvement of the detection limit by the proper scan rate.

4.4 Conclusion

In conclusion, a new method to measure the H_2 evolution reaction is demonstrated by P-ECi technique. In this method, H^+ concentration change near the metal substrate surface are driven by apply voltage to the surface, and the change is detected from the P-ECi images. The pH indicator increases the refractive index change due to the color change with H^+ changing, leading to a 2 times signal enhancement for detection of the H_2 evolution reaction. Because many biological and chemical reactions are related with H^+ changing, the method could be used for high throughput analysis of H^+.

CHAPTER 5 CONCLUSION AND FUTURE WORK

Microscope technique has been developed for more than 400 years. The goal of the most type of microscopes is to measure the morphology or optical properties of the sample. The invention of scanning tunneling microscope (STM), atomic force microscope (AFM), and transmission electron microscope (TEM) expands the microscope to the resolution range from angstrom to millimeter. This thesis discussed the combination of the plasmonic based microscope with EC measurement to provide the chemical reaction information of the surface.

SECM is a kind of method to obtain local EC properties of the surface. However, it needs microelectrodes to scan the sensing surface. The scanning microelectrode will perturb the reaction when the distance between electrode and sensing surface is within diffusion length of reaction. The other disadvantage is that the scalability of SECM has to be scaled down by smaller electrode. Recently, the P-ECi method has been developed to overcome the obstacles of SECM. The P-ECi method measures current by the SPR images which is accompanied with EC process current. In this thesis, we expand a new aspect of the P-ECi technique into thin film microfluidic system. Besides, a universal algorithm has been developed to calculate EC current from P-ECi response signal. Another application based on P-ECi method is demonstrated to enhanced the detection of imaging catalytic current on platinum nanoparticle.

Gaining more insights into the correlation between the SPR imaging and EC current characteristics will benefit the application and improvement of P-ECi technique. P-ECi technique is useful for different applications which need local EC information. For

example, detection of DNA and protein array and cell based detection are promising applications. Further, based on the results in Chapter 4, it is possible to detect the EC reaction on single nanoparticle by P-ECi technique. As the P-ECi technique will inevitability matured and improved, more and more applications based on P-ECi will begin.

REFERENCES

[1] S. Wang, *et al.*, "Electrochemical Surface Plasmon Resonance: Basic Formalism and Experimental Validation," *Analytical Chemistry*, vol. 82, pp. 935-941, 2010/02/01 2010.

[2] X. Shan, *et al.*, "Imaging Local Electrochemical Current via Surface Plasmon Resonance," *Science*, vol. 327, pp. 1363-1366, March 12, 2010 2010.

[3] A. Bratov, *et al.*, "Recent trends in potentiometric sensor arrays—A review," *Analytica Chimica Acta*, vol. 678, pp. 149-159, 2010.

[4] V. K. Gupta, *et al.*, "Voltammetric techniques for the assay of pharmaceuticals—A review," *Analytical Biochemistry*, vol. 408, pp. 179-196, 2011.

[5] C. Amatore, *et al.*, "Simultaneous Detection of Reactive Oxygen and Nitrogen Species Released by a Single Macrophage by Triple Potential-Step Chronoamperometry," *Analytical Chemistry*, vol. 82, pp. 1411-1419, 2010/02/15 2010.

[6] S. Hartwell and K. Grudpan, "Flow based immuno/bioassay and trends in micro-immuno/biosensors," *Microchimica Acta*, vol. 169, pp. 201-220, 2010/06/01 2010.

[7] Y. Shao, *et al.*, "Graphene Based Electrochemical Sensors and Biosensors: A Review," *Electroanalysis*, vol. 22, pp. 1027-1036, 2010.

[8] D. W. Kimmel, *et al.*, "Electrochemical Sensors and Biosensors," *Analytical Chemistry*, vol. 84, pp. 685-707, 2012/01/17 2011.

[9] M. Yang, *et al.*, "Cell Docking and On-Chip Monitoring of Cellular Reactions with a Controlled Concentration Gradient on a Microfluidic Device," *Analytical Chemistry*, vol. 74, pp. 3991-4001, 2002/08/01 2002.

[10] T. Gervais and K. F. Jensen, "Mass transport and surface reactions in microfluidic systems," *Chemical Engineering Science*, vol. 61, pp. 1102-1121, 2006.

[11] H. Andersson and A. van den Berg, "Microfluidic devices for cellomics: a review," *Sensors and Actuators B: Chemical*, vol. 92, pp. 315-325, 2003.

[12] S. K. Sia and G. M. Whitesides, "Microfluidic devices fabricated in Poly(dimethylsiloxane) for biological studies," *ELECTROPHORESIS*, vol. 24, pp. 3563-3576, 2003.

[13] S. C. Jacobson, *et al.*, "Microfluidic Devices for Electrokinetically Driven Parallel and Serial Mixing," *Analytical Chemistry*, vol. 71, pp. 4455-4459, 1999/10/01 1999.

[14] M. P. C. Marques and P. Fernandes, "Microfluidic Devices: Useful Tools for Bioprocess Intensification," *Molecules*, vol. 16, pp. 8368-8401, 2011.

[15] K.-K. Liu, *et al.*, "Microfluidic Systems for Biosensing," *Sensors*, vol. 10, pp. 6623-6661, 2010.

[16] A. Bard and L. Faulkner, *Electrochemical Methods: Fundamentals and Applications*: John Wiley & Sons, Inc, 2001.

[17] W. Knoll, "Interfaces and thin films as seen by bound electromagnetic waves," *Annual Revies of Physical Chemistry*, vol. 49, pp. 569-638, 1998.

[18] H. Raether, "Surface plasma oscillations and their applications," *Physics of thin film*, vol. 9, pp. 145-261, 1977.

[19] H. Raether, Ed., *Surface plasmons on smooth and rough surfaces and gratings*. New York: Springer-Berlag, 1986, p.^pp. Pages.

[20] A. Otto, "Excitation of naoradiative surface plasma waves in silver by the method of frustrated total reflection," *Zeitschrift für Physik*, vol. 216, pp. 398-410, 1968.

[21] E. Kretschmann, "The ATR Method with Focused Ligh-application to Guided Waves on a Grating," *Optics Communications*, vol. 26, pp. 41-44, 1978.

[22] Biacore, "Surface Plasmon Resonance," September 2001.

[23] H. J. Lee, *et al.*, "SPR Imaging Measurements of 1-D and 2-D DNA Microarrays Created from Microfluidic Channels on Gold Thin Films," *Analytical Chemistry*, vol. 73, pp. 5525-5531, 2001/11/01 2001.

[24] G. J. Wegner, *et al.*, "Real-Time Surface Plasmon Resonance Imaging Measurements for the Multiplexed Determination of Protein Adsorption/Desorption Kinetics and Surface Enzymatic Reactions on Peptide Microarrays," *Analytical Chemistry*, vol. 76, pp. 5677-5684, 2004/10/01 2004.

[25] Y. Iwasaki, *et al.*, "Electrochemical reaction of Fe(CN)3−/4−6 on gold electrodes analyzed by surface plasmon resonance," *Surface Science*, vol. 427–428, pp. 195-198, 1999.

[26] S. Wang, *et al.*, "Detection of Heavy Metal Ions in Water by High-Resolution Surface Plasmon Resonance Spectroscopy Combined with Anodic Stripping Voltammetry," *Analytical Chemistry*, vol. 79, pp. 4427-4432, 2007/06/01 2007.

[27] S. Wang, *et al.*, "Surface plasmon resonance enhanced optical absorption spectroscopy for studying molecular adsorbates," *Review of Scientific Instruments*, vol. 72, pp. 3055-3060, 2001.

[28] S. Wang, *et al.*, "High-Sensitivity Stark Spectroscopy Obtained by Surface Plasmon Resonance Measurement," *Analytical Chemistry*, vol. 72, pp. 4003-4008, 2000/09/01 2000.

[29] X. Kang, *et al.*, "A novel electrochemical SPR biosensor," *Electrochemistry Communications*, vol. 3, pp. 489-493, 2001.

[30] R. Schweiss, *et al.*, "Electropolymerization of ethylene dioxythiophene (EDOT) in micellar aqueous solutions studied by electrochemical quartz crystal microbalance and surface plasmon resonance," *Electrochimica Acta*, vol. 50, pp. 2849-2856, 2005.

[31] S. Kienle, *et al.*, "Electropolymerization of a phenol-modified peptide for use in receptor–ligand interactions studied by surface plasmon resonance," *Biosensors and Bioelectronics*, vol. 12, pp. 779-786, 1997.

[32] A. J. BARD, *et al.*, "Chemical Imaging of Surfaces with the Scanning Electrochemical Microscope," *Science*, vol. 254, pp. 68-74, October 4, 1991 1991.

[33] M. J. Jory, *et al.*, "A surface-plasmon-based optical sensor using acousto-optics," *Measurement Science and Technology*, vol. 6, p. 1193, 1995.

[34] C. R. Lawrence, *et al.*, "Surface plasmon resonance studies of immunoreactions utilizing disposable diffraction gratings," *Biosensors and Bioelectronics*, vol. 11, pp. 389-400, 1996.

[35] X. Shan, *et al.*, "A label-free optical detection method for biosensors and microfluidics," *Applied Physics Letters*, vol. 92, pp. 133901-3, 2008.

[36] K. J. Foley, *et al.*, "Surface Impedance Imaging Technique," *Analytical Chemistry*, vol. 80, pp. 5146-5151, 2008/07/01 2008.

[37] M. Ferrari, "Cancer nanotechnology: opportunities and challenges," *sNature Review Cancer*, vol. 5, pp. 161-171, 2005.

[38] F. Patolsky, *et al.*, "Nanowire-Based Biosensors," *Analytical Chemistry*, vol. 78, pp. 4260-4269, 2006/07/01 2006.

[39] W. U. Wang, *et al.*, "Label-free detection of small-molecule–protein interactions by using nanowire nanosensors," *Proceedings of the National Academy of Sciences of the United States of America*, vol. 102, pp. 3208-3212, March 1, 2005 2005.

[40] Z. Li, *et al.*, "Silicon nanowires for sequence-specific DNA sensing: device fabrication and simulation," *Applied Physics A*, vol. 80, pp. 1257-1263, 2005/03/01 2005.

[41] F. Patolsky, *et al.*, "Electrical detection of single viruses," *Proceedings of the National Academy of Sciences of the United States of America*, vol. 101, pp. 14017-14022, September 28, 2004 2004.

[42] Q. W. Y. Cui, H. Park, and C. M. Lieber, "Nanowire Nanosensors for Highly Sensitive and Selectrive Detection of Biological and Chemical Species," *Science*, vol. 17, pp. 1289-1292, 2001.

[43] P. G. Collins, *et al.*, "Extreme Oxygen Sensitivity of Electronic Properties of Carbon Nanotubes," *Science*, vol. 287, pp. 1801-1804, March 10, 2000 2000.

[44] Y. X. Liang, *et al.*, "Low-resistance gas sensors fabricated from multiwalled carbon nanotubes coated with a thin tin oxide layer," *Applied Physics Letters*, vol. 85, pp. 666-668, 2004.

[45] M. E. Stewart, *et al.*, "Nanostructured Plasmonic Sensors," *Chemical Reviews*, vol. 108, pp. 494-521, 2008/02/01 2008.

[46] A. D. McFarland and R. P. Van Duyne, "Single Silver Nanoparticles as Real-Time Optical Sensors with Zeptomole Sensitivity," *Nano Letters*, vol. 3, pp. 1057-1062, 2003/08/01 2003.

[47] Y. T. J. Zhang, K. Lee, and M. Ouyang, "Tailoring Light-matter-spin Interactions in Colloidal Hetero-nanostructures," *Nature*, vol. 466, pp. 91-95, 2010.

[48] N. Tian, *et al.*, "Synthesis of Tetrahexahedral Platinum Nanocrystals with High-Index Facets and High Electro-Oxidation Activity," *Science*, vol. 316, pp. 732-735, May 4, 2007 2007.

[49] A. Z. Moshfegh, "Nanoparticle catalysts," *Journal of Physics D: Applied Physics*, vol. 42, p. 233001, 2009.

[50] C. M. Sánchez-Sánchez, *et al.*, "Imaging Structure Sensitive Catalysis on Different Shape-Controlled Platinum Nanoparticles," *Journal of the American Chemical Society*, vol. 132, pp. 5622-5624, 2010/04/28 2010.